AIAA JOURNAL
Vol. 48, No. 2, February 2010

Burning Velocities of Alternative Gaseous Fuels at Elevated Temperature and Pressure

A. Bagdanavicius,* P. J. Bowen,† N. Syred,‡ P. Kay,§ and A. Crayford¶
Cardiff University, Cardiff, Wales CF24 3AA, United Kingdom
and
G. Sims** and J. Wood††
QinetiQ, Farnborough, England GU14 0LX, United Kingdom

DOI: 10.2514/1.43225

This study has been undertaken to investigate turbulent burning velocities of alternative gaseous fuels at elevated temperature and pressure using the established Bunsen burner method. The experiments were conducted in the industrial scale high-pressure optical chamber at the Gas Turbine Research Centre of Cardiff University. Five different gaseous fuels, methane, two methane–carbon dioxide mixtures, and two methane–hydrogen mixtures were studied. Experiments were conducted at two different temperatures (473 K and 673 K) and two different pressures (3 bara and 7 bara). Analysis of measurements made using 100% methane showed anticipated burning velocity trends with variation in temperature and pressure. The results reported here showed reasonable agreement with the available turbulent burning velocity correlations, although the burning velocities recorded by the other researchers were somewhat higher. The stoichiometric flames considered were all purposely contained within one flame regime on the Borghi–Peters diagram, namely the corrugated flamelet regime, through appropriate choice of operating conditions. Hydrogen enrichment and carbon dioxide dilution of methane show some expected trends. As expected, dilution of methane with carbon dioxide reduces the measured burning velocity. However, increasing pressure and temperature in this case have competing effects, with temperature raising the burning velocity and pressure reducing it. Comparison of the methane–carbon dioxide mixture results presented here are consistent with the qualitative trends recently reported by the group of researchers, but exhibit quantitative differences thought to be due to experimental and data analysis differences. Hydrogen enrichment of the methane leads to a significant increase in the measured burning velocity compared with methane, as anticipated. Comparison of the methane–hydrogen mixture results reported here show reasonable agreement with the measurements of other researchers. Our measurements show that increases in temperature and pressure independently lead to increased turbulent burning velocity, with a more pronounced effect of pressure for lean flames.

Nomenclature

A	=	flame area, m^2
a, b	=	fraction ratio
D_{10}	=	arithmetic mean diameter
h	=	pixel height, mm
l_0	=	integral length scale, m
k	=	number of pixel rows in the image
Le	=	Lewis number
M	=	molar mass, g/mol
$\dot{m}$	=	mass flow rate, kg/s
n	=	number of pixels
q'	=	averaged turbulence intensity, m/s
$R(\tau)$	=	autocorrelation function
r	=	burner radial position, mm
S_L	=	laminar burning velocity, m/s
S_T	=	turbulent burning velocity, m/s
u, v	=	instantaneous axial and radial velocity, m/s
$\bar{u}$, $\bar{v}$	=	mean axial and radial velocity, m/s
u', v'	=	fluctuating axial and radial velocity component, m/s
u_{rms}, v_{rms}	=	axial and radial turbulence intensity, m/s
$\dot{V}$	=	volume flow rate, m^3/s
w	=	pixel width, mm
X	=	molar fraction
Y	=	mass fraction
δ_L	=	laminar flame thickness, mm
τ_0	=	integral time scale, s
τ	=	lag time, s
ρ	=	density, kg/m^3
$\rho(\tau)$	=	autocorrelation coefficient
ϕ	=	equivalence ratio
R	=	reactants
rms	=	root mean square
st	=	stoichiometric

Presented as Paper 0229 at the 47th Aerospace Sciences Meeting, Orlando World Center Marriott, Orlando, FL, 5–8 January 2009; received 14 January 2009; revision received 1 October 2009; accepted for publication 3 November 2009.

*Marie Curie Researcher, Cardiff School of Engineering, The Parade. Member AIAA.
†Professor, Cardiff School of Engineering, The Parade.
‡Professor, Cardiff School of Engineering. Member AIAA.
§Research Associate, Cardiff School of Engineering.
¶Research Associate, Cardiff School of Engineering.
**Cody Technology Park, Ively Road.
††Cody Technology Park, Ively Road.

I. Introduction

INDUSTRIAL gas turbines have been increasingly used for a wide range of power generation and mechanical drive applications. However, with growing concerns regarding global warming and energy security, a new range of alternative fuels are being considered for use in such devices. Such fuels can be divided broadly into two groups, those containing methane diluted with an inert gas, often carbon dioxide in bioderived fuels, and those containing methane enriched with hydrogen. Environmental constraints for gas turbines

Table 1 Investigated gas mixtures

Gas mixture	CH_4, %	CO_2, %	H_2, %	Pressure, bara	Temperature, K
100%CH_4	100	0	0	3, 7	473, 673
85%CH_4-15%CO_2	85	15	0	3, 7	473, 673
70%CH_4-30%CO_2	70	30	0	3, 7	473, 673
85%CH_4 -15%H_2	85	0	15	3, 7	473, 673
70%CH_4-30%H_2	70	0	30	3, 7	473, 673

mean that NO_x production must also be considered, implying that such fuels should be burnt using current lean premixed technology. A key parameter in the design of such systems, influencing flame stability and position, is the turbulent burning velocity.

The current study has been undertaken to investigate turbulent burning velocities of gaseous fuel mixtures with significant carbon dioxide dilution or hydrogen enrichment at elevated temperature and pressure using the established Bunsen burner method. The test program has been carried out on behalf of a 23-partner European Union program [1]. The aim of this work is to add to the understanding of the turbulent burning velocities of alternative fuels over a range of equivalence ratios, temperatures, and pressures.

There have been many attempts to investigate laminar and turbulent methane flames [2,3], methane and carbon dioxide mixtures [4], methane and hydrogen mixtures [5–9], and even synthetic gas fuel mixtures [10] at atmospheric and nonatmospheric conditions.

Laminar methane flames were investigated by Egolfopoulus et al. [2] under both reduced and elevated pressures using counterflow flame methodologies. Their study illustrated the influence of pressure on the laminar burning velocity, which decreases with increasing pressure. Kobayashi [3] investigated turbulent flames using a Bunsen burner technique and showed that turbulent and laminar flame ratio S_T/S_L is pressure dependant and rises with increasing pressure. The study also showed that flame shape becomes more wrinkled at higher pressures.

The effect of carbon dioxide dilution on turbulent premixed flames was studied by Kobayashi et al. [4] using the Bunsen burner technique at elevated pressure and temperature. They reported that S_T/S_L decreased when air was diluted with CO_2 at 5 bara 573 K. This counterintuitive result is explained principally through the effect of local flame stretch that reduces local burning velocity.

Burning rates of methane and hydrogen mixtures have been investigated previously, though few at elevated ambient conditions. Mandilas et al. [8] performed turbulent premixed flame experiments in a combustion chamber at 5 bara pressure with 5% of hydrogen by mass added to methane. The peak burning velocity occurred at $\phi = 0.85$. They concluded that hydrogen addition has a larger effect on burning velocity for lean flames and little effect for rich flames. A Bunsen burner type flame was used in the experiments of Halter et al. [6] to investigate turbulent premixed methane–hydrogen flames. An increase in S_T/S_L with hydrogen addition for elevated pressures of 3 and 5 bar was observed.

Several different methods have been used previously to identify the flame front of Bunsen-type burner premixed turbulent flames. A popular approach to identify the average flame front is to superimpose raw flame images [3,11] and calculate the threshold based on the ensemble average of the mean and maximum signal intensities [12].

Another common technique is to binarize raw images using bimodal intensity histograms [13] or to define the image conversion threshold value using manual or automatic methods. These binary images are subsequently averaged. The burning velocity can then be calculated using the flame cone angle method [14] or by rotating the averaged image around its central axis [11]. Most of the methods found in the literature rely on flame averaging. This flame-averaging technique, the so-called averaged flame shape method, was initially applied to calculate the average flame front area for the current data set. However, another method called the average flame area technique was developed to process images and is considered more reliable in this study, hence used throughout.

II. Experimental Methodology

In this experimental program, five different gaseous fuels were tested over a range of pressures and temperatures. Approximately 20 data sets were generated for each gas mixture[‡‡]: 100% methane, 85% methane–15% carbon dioxide, 70% methane–30% carbon dioxide, 85% methane–15% hydrogen, and 70% methane–30% hydrogen were carried out for lean and rich mixtures from 0.65 to 1.45 equivalence ratio at different pressures and temperatures (Table 1).

A. Test Facility

The tests were performed in the high-pressure optical chamber (HPOC) integrated within the high-pressure combustion rig, which is located at the Gas Turbine Research Centre of Cardiff University in Port Talbot, Wales, United Kingdom.

The HPOC consists of a horizontally mounted burner firing into an inner combustion chamber, enclosed within an optical pressure casing. The HPOC can operate with working pressures of up to 16 bara and inlet temperatures of up to 900 K. The pressure casing is a cylindrical geometry with four opposed quartz windows, affording excellent optical access (Fig. 1).

The optical combustion section is connected to a compressor and heat exchanger, allowing combustion air to be preheated to required operating temperatures. The inner combustion chamber is of rectangular form and has four internal quartz windows that align with the outer casing, giving full optical access to the combustion chamber. The width and height of the combustion chamber is 150 mm. The inner combustion chamber is constructed from aerograde stainless steel sheet, allowing (if required) external cooling air to pass into the combustion chamber, mimicking the behavior of practical gas turbine combustors. The flame is thus confined to the combustion chamber. The internal windows are continuously purged with air during the tests to ensure they are kept clear of any deposits of seed. Extensive experience with the rig shows that the windows' purge has little effect on measured values. A simple Bunsen-type burner is fired into the combustion chamber (diameter 25 mm). The burner is fitted with an annular pilot that supplies a methane diffusion flame to aid stability while adjusting the operating conditions. This pilot is switched off before making measurements.

The main burner is fed a premix of fuel and air via a turbulence mixing plate, 50 mm in diameter, with 53 holes each of 1.5 mm diameter and blockage ratio 95%. This creates uniform turbulence and aids in the mixing of the reactants. The fuel gas supply is connected to a mixing chamber upstream of this plate. Preheated air for combustion, which is seeded with aluminum oxide particles[§§], is delivered through the preheater to the top of the mixing chamber of the burner. A more detailed burner and combustor geometry is presented in Fig. 2.

The air supply for both the HPOC and burner is pressurized by the main facility compressor, which is capable of delivering 5 kg/s at 16 bar pressure. Seeded air for combustion is delivered by an auxiliary compressor. Fuel gases are supplied from premixed cylinders. The overall scheme for the rig is shown in Fig. 3.

Two different measurement techniques were applied. First, a nonintrusive 2-D laser diagnostic technique, laser Doppler anemometry (LDA), was used to determine both the velocity profile and

[‡‡]all by volume

[§§]Size $D_{10} < 1$ μm

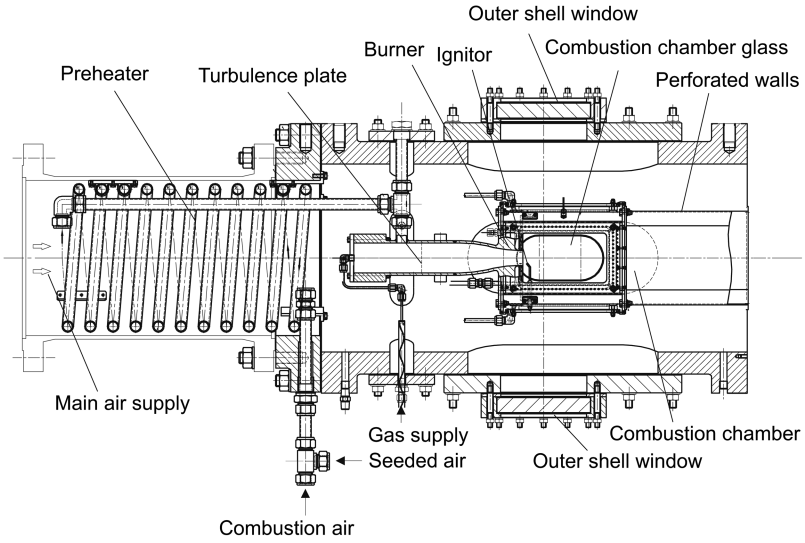

Fig. 1 Cross section of the HPOC.

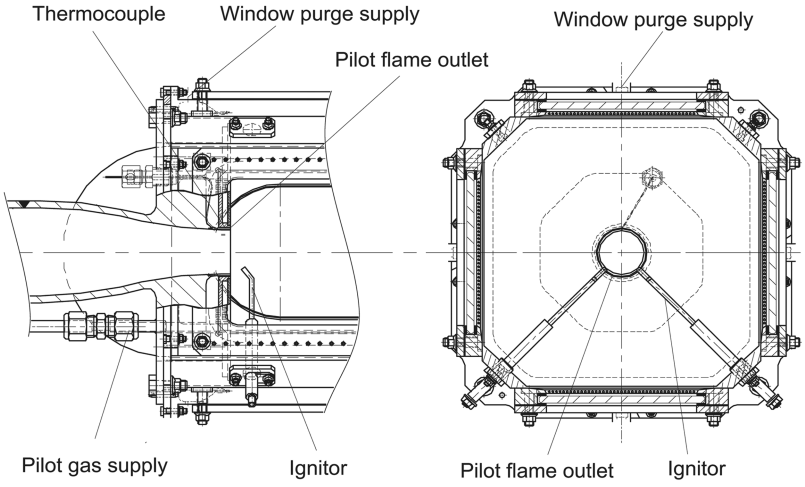

Fig. 2 Detailed combustor geometry.

turbulence characteristics at the exit of the burner at elevated pressures and temperatures. A Dantec laser system was used for this purpose. Secondly, planar laser tomography was applied to measure the turbulent burning velocity for the different gas mixtures at a range of temperatures and pressures. Images of the flame front were recorded using a Photron APX-rs high-speed camera mounted perpendicularly and synchronized with a pulsed (Nd:YAG) sheet laser. To ensure reliability for each test, 1000 images were recorded at 10 Hz.

The experiments were run and monitored from a remote control room. LDA and laser planar tomography systems were controlled from their own dedicated computers, and the facility was controlled

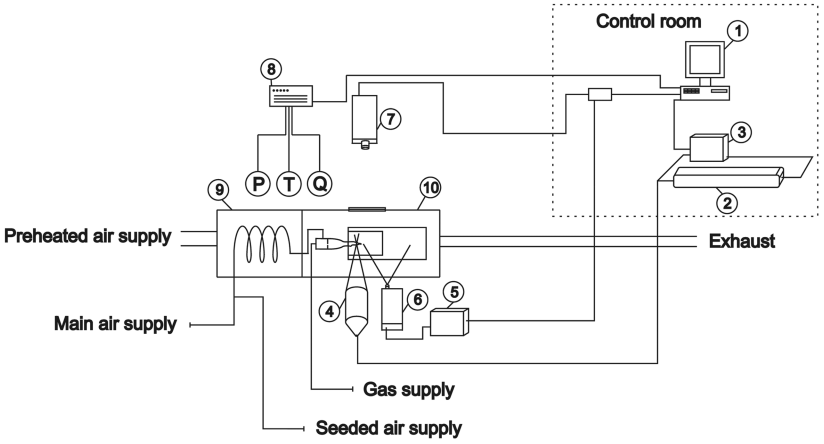

Fig. 3 Experimental setup. 1) Data acquisition and laser control system, 2) LDA laser, 3) LDA laser processor, 4) LDA laser probe, 5) sheet laser controller, 6) sheet laser, 7) high-speed digital camera, 8) data logger, 9) combustion air preheater, and 10) high-pressure optical combustor.

from its own programmable logic controller system. Fuel, combustion air, and seed air were measured simultaneously using suitably ranged Coriolis flow meters. All experimental conditions, such as pressure, temperature, air flow, and gas flow were recorded by a facility data acquisition system. Measured temperatures and pressures were reasonably steady with fluctuations not exceeding 5% and 3% of the nominal values for pressure and temperature, respectively.

B. Calculation Method

General stoichiometric combustion reactions for methane, methane–carbon dioxide, and methane–hydrogen gas mixtures, based on methane gas, can be written as follows:

$$\mathrm{CH_4} + 2 \cdot (\mathrm{O_2} + 3.76 \cdot \mathrm{N_2}) = \mathrm{CO_2} + 2 \cdot \mathrm{H_2O} + 2 \cdot 3.76 \cdot \mathrm{N_2} \tag{1}$$

$$\mathrm{CH_4} + a \cdot \mathrm{CO_2} + 2 \cdot (\mathrm{O_2} + 3.76 \cdot \mathrm{N_2}) = (a+1) \cdot \mathrm{CO_2} + 2 \cdot \mathrm{H_2O} + 2 \cdot 3.76 \cdot \mathrm{N_2} \tag{2}$$

$$\mathrm{CH_4} + b \cdot \mathrm{H_2} + \left(\frac{b+4}{2}\right) \cdot (\mathrm{O_2} + 3.76 \cdot \mathrm{N_2}) = \mathrm{CO_2} + (b+2) \cdot \mathrm{H_2O} + \left(\frac{b+4}{2}\right) \cdot 3.76 \cdot \mathrm{N_2} \tag{3}$$

Here a and b are the molar fraction ratios of additional gas in methane, $a = X_{\mathrm{CO_2}}/X_{\mathrm{CH_4}}$ and $b = X_{\mathrm{H_2}}/X_{\mathrm{CH_4}}$.

Stoichiometric air fuel ratios (AFR) of methane, methane–carbon dioxide, and methane–hydrogen mixtures are calculated

$$\mathrm{AFR}_{\mathrm{st}}^{\mathrm{CH_4}} = \frac{2 \cdot (M_{\mathrm{O_2}} + 3.76 \cdot M_{\mathrm{N_2}})}{M_{\mathrm{CH_4}}} \tag{4}$$

$$\mathrm{AFR}_{\mathrm{st}}^{\mathrm{CH_4-CO_2}} = \frac{2 \cdot (M_{\mathrm{O_2}} + 3.76 \cdot M_{\mathrm{N_2}})}{M_{\mathrm{CH_4}} + a \cdot M_{\mathrm{CO_2}}} \tag{5}$$

$$\mathrm{AFR}_{\mathrm{st}}^{\mathrm{CH_4-H_2}} = \frac{\left(\frac{b+4}{2}\right) \cdot (M_{\mathrm{O_2}} + 3.76 \cdot M_{\mathrm{N_2}})}{M_{\mathrm{CH_4}} + b \cdot M_{\mathrm{H_2}}} \tag{6}$$

The mass flow rate of gas mixture and air is measured and the equivalence ratio is calculated thus:

$$\phi = \frac{\mathrm{AFR_{st}}}{\dot{m}_{\mathrm{air}}/\dot{m}_{\mathrm{fuel}}} \tag{7}$$

The tests were performed using a Bunsen-type burner. Thus, the tested flames were envelope-category flames. This means that the flame forms an envelope around the reactants and all reactants must pass through the flame [15]. Thus, the burning velocity is related to global consumption speed [16] and is calculated by the formula

$$S_T = \frac{\dot{m}_R}{\rho_R \cdot A} = \frac{\dot{V}}{A} \tag{8}$$

It has been proposed that the consumption speed should be used to define the turbulent burning velocity [17] and that only flames within a particular category should be compared because the flame wrinkling process can be different for different flame types [18]. However, in our study we compared envelope-category flames as well as spherical-type flames, due to the lack of research performed at elevated pressures and temperatures for the studied gas mixtures.

The exit velocity from the burner of the gas–air mixture is derived from the mass flow of combustion air, seed air, and fuel flows, and displayed and logged simultaneously by the data acquisition system. Density, viscosity, diffusion coefficients, and other gas properties of the combustible mixture at the required temperature and pressure were calculated using polynomial fit coefficients available within the CHEMKIN database or taken from reference tables. Lewis number, defined as the ratio of thermal diffusivity of the mixture and mass diffusivity of deficient species, was calculated for all mixtures considered.

The CHEMKIN-PRO software and GRI-Mech 3.0 reaction mechanism were used to calculate laminar burning velocities and flame thicknesses for the various gas mixtures at different pressures, temperatures, and equivalence ratios. The laminar flame thickness calculation method was based on a classical approach of defining temperature gradient and agreed well with findings of Lafay et al. [19], who made hydrogen enriched methane–air flame thickness measurements. These results support the computational results obtained using the GRI-Mech 3.0 reaction mechanism for equivalence ratios above 0.55.

C. Measurement Technique

The LDA results were used to ensure that turbulence intensity and burner exit velocity profiles were uniform and to find integral time scales of turbulence. The velocity and turbulence profiles of isothermal air flow, seeded with aluminum oxide particles, were measured 10 mm downstream of the burner exit across the burner axis on the centerline plane. The axial and radial velocities were recorded for a range of exit velocities at ambient pressures of 3 and 7 bara and temperatures of 473 K to 673 K. LDA data processing was carried out using DANTEC Flow manager software. The autocorrelation coefficient $\rho(\tau)$ was calculated thus:

$$\rho(\tau) = \frac{R(\tau)}{R(0)} = \frac{\overline{u'(t)u'(t+\tau)}}{u_{\mathrm{rms}}^2} \tag{9}$$

where τ is the time lag, $R(0)$ is the correlation estimated at lag time zero, and $R(\tau)$ is the estimated correlation. From the autocorrelation coefficient the integral time scale τ_0 was found

$$\tau_0 = \int_0^\infty \rho(\tau)\, \mathrm{d}\tau \tag{10}$$

Then assuming that the field has uniform mean velocity and accepting Taylor's hypothesis the integral length scale can be computed from the formula

$$l_0 = \bar{u} \cdot \tau_0 \tag{11}$$

It was assumed that the flow is statistically axisymetric, and therefore, radial and circumferential rms velocities are equal, thus the total turbulence intensity can be calculated

$$q' = \sqrt{\frac{u_{\mathrm{rms}}^2 + 2 \cdot v_{\mathrm{rms}}^2}{3}} \tag{12}$$

Measured velocities and turbulence characteristics data of isothermal air flow at different conditions later have been used to define velocities and turbulence parameters for every particular gas mixture.

D. Flame Imaging

The planar laser tomography technique used in this study is based on the observation that the density of the products is lower than that of the reactants. Consequently when the uniformly seeded reactants are converted to products the seed density reduces and the scattered light intensity falls. As the flame thickness is small, a clear demarcation is generated between products and reactants that can be identified as the flame front.

First, all raw flame images are averaged (Fig. 4a,) using a bespoke MATLAB script. Then a set of the background images (taken at the end of the test when the flame is no longer present) are averaged using the same image processing technique (Fig. 4b). The average background image is then subtracted from the average flame front image (Fig. 4c). The average flame front image is converted to the binary image using a defined threshold value (Fig. 4d).

However, the averaged flame shape method based on raw images is reliant on user interpretation of the results before defining the threshold value, which could introduce systematic errors. Also, it

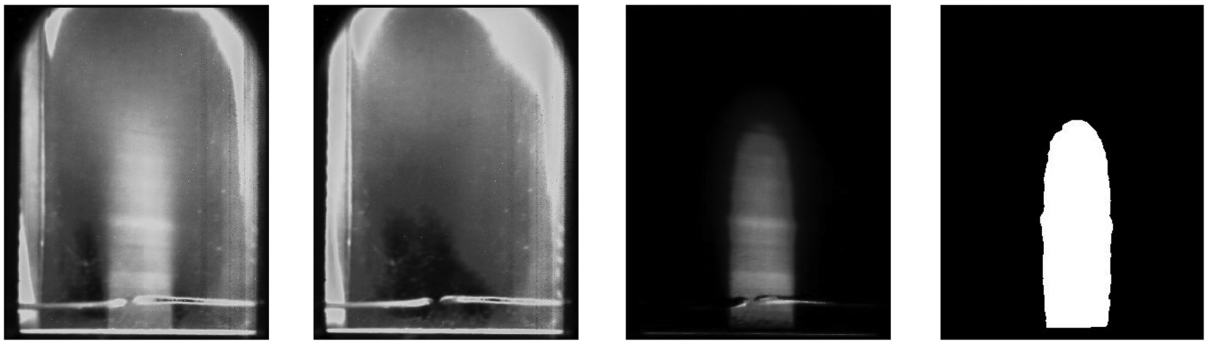

a) b) c) d)

Fig. 4 Averaged flame shape method based on raw images: a) averaged flame image, b) averaged background image, c) averaged flame image background subtracted, and d) converted binary image.

was observed that the flame front was very irregular in shape for all experiments independent of pressure and temperature. Hence, this technique is considered unrepresentative for calculating the average flame front area from the average flame shape based on raw flame images.

As is seen from the image (Fig. 4c), due to the different levels of light, the conversion from a grayscale image to the binary image could be misinterpreted. Although the threshold value can be selected manually or automatically using an image processing technique, subjectivity cannot be eliminated. Hence, a more robust method for calculating the area of the flame front was developed, called the averaged flame area method.

In this method, the area of each single flame image was calculated using MATLAB. First, each individual image was filtered using morphological image processing techniques and median filters, and the background subtracted. Subsequently the grayscale image is converted into a binary image using manually selected threshold values. Different threshold values are required for each test case, due to the variance of background noise and seed rates. After conversion of the grayscale images (Fig. 5) to the binary images (Fig. 6) the pixels of the flame area of every single image are counted and flame area calculated.

Flame area of each individual flame image is calculated using

$$A = \sum_{1}^{k} (\pi \cdot n_k \cdot h \cdot w) \tag{13}$$

Here n is the number of pixels, h is the pixel height 0.353 mm, and w is pixel width 0.353 mm; the pixel height and width were found by imaging a scale within the test section. To calculate the flame area each row of pixels within the image was then rotated around its own centerline axis. The side area of every cylinder made of pixels was calculated and summed. It was found by applying this method that there was substantial frame to frame variation in the surface area of the flames at a single operating point. To calculate the average turbulent burning velocity for each condition the statistical software MINITAB was applied. Using this approach it was possible to identify and reject all results that were outside the limit of two standard deviations. A new mean flame area could then be found and finally the turbulent burning velocity calculated.

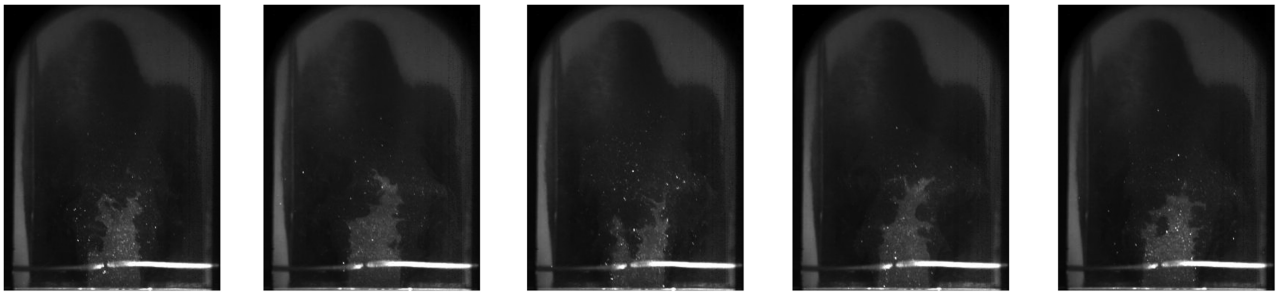

Fig. 5 Raw methane–hydrogen mixture flame images.

Fig. 6 Processed binary methane–hydrogen mixture flame images.

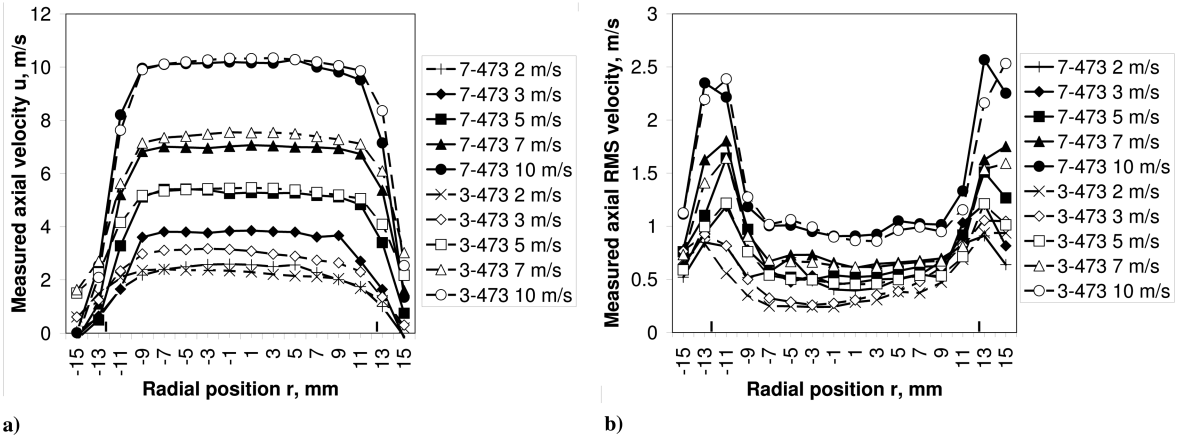

a) b)

Fig. 7 Axial mean velocity $\bar{u}$ and axial rms velocity u_{rms} measured 10 mm downstream burner exit at different bulk gas flow velocities. Velocities indicated in the legend represents bulk exit velocity at 3 bara 473 K (3–473) and 7 bara 473 K (7–473): a) axial mean velocity, and b) axial rms velocity.

III. Results and Discussion

A. Isothermal Laser Doppler Anemometry Results

Figure 7 shows the variation of mean axial velocity and velocity fluctuations, respectively, with radial position for a range of exit velocities. The two vertical lines at radial position $r = 12.5$ mm and $r = -12.5$ mm represent the burner edges. Overall the results show that the axial velocity profiles are uniform, confirming the suitability of the burner for this study. Pressure has little effect on axial velocity and axial velocity fluctuations.

Using LDA, 5000 samples were collected at each position across the center of the burner (radial position $r = -9 \div 9$ mm) at each condition. Because of the flow stream shape the seeding rate was somewhat lower at the edges of the burner ($r = 9 \div 13$ mm). The relative error did not reach 0.5% for the measurements in the center of the burner and did not exceed 3% for the measurements at the edges of the burner. The data validation rate was above 90% during all tests.

LDA measurements of the isothermal flow showed that, in agreement with others [20], turbulence intensity is almost insensitive to variation in pressure and temperature. Figure 8 shows that the turbulence intensity q' measured at the burner radial position $r =$ 12 mm shows a dependence on bulk-flow velocity. During the experiments bulk exit velocity varied between 4 to 16 m/s and thus, turbulence intensity values at different bulk flow velocities were interpolated from this correlation.

The evolution of relative turbulence intensity as a function of bulk flow velocity is represented in Fig. 9. The increase in relative turbulence intensity $q'/\bar{u}$ at low bulk flow velocities is clearly seen from the graph.

Data obtained by LDA were used to derive one point temporal velocity correlation and calculate the integral time scale and integral length scale of the turbulent isothermal flow at different pressures, temperatures, and bulk flow velocities. One thousand and twenty-four correlation samples and a lag time $\tau = 100$ ms were chosen to find autocorrelation coefficients. The integral time scale was found by integrating the autocorrelation function over time. The integral length scale was calculated using formula Eq. (11), based on Taylor's hypothesis of isotropic turbulence. As this frozen-turbulence hypothesis is a good approximation only if $q'/\bar{u} \ll 1$, the calculation of integral time scale should only be performed where the velocity fluctuation is relatively low [21]. Two-point spatial velocity correlation should be carried out to calculate integral time scale where stronger turbulence prevails. Spatial and temporal correlation agree well for low turbulence flows, and strong streamline development of turbulence invalidates the frozen-turbulence assumption of Taylor's hypothesis [22].

Typical autocorrelation function curves are represented in Fig. 10. It was found that at 10 m/s bulk exit velocity at 7 bara, 473 K, and 673 K conditions, few data points around the center of burner exit correlated, and others oscillated and did not cross zero. The same behavior was observed processing LDA data taken from the data points close to the burner rim ($r \approx 12$ mm). This could be due to increased normalized turbulence intensity (relative turbulence intensity) $q'/\bar{u}$ invalidating Taylor's frozen-turbulence theory. This data for this condition is not typical.

Averaged integral length scale data obtained from autocorrelation coefficients measured at a different burner radial position $r < 5$ mm are presented in Fig. 11. Only correlated values have been used to process integral time scale and length scale. The data are consistent at 3 bara 473 K conditions for all exit velocities. In this case the integral length scale l_0 is between 5 to 13 mm. At 3 bara 673 K the integral length scale increases up to 15 mm. At 7 bara pressure the integral length scale reduces to a maximum of 10 mm for all exit velocities except for the aforementioned 10 m/s exit velocity case. For the

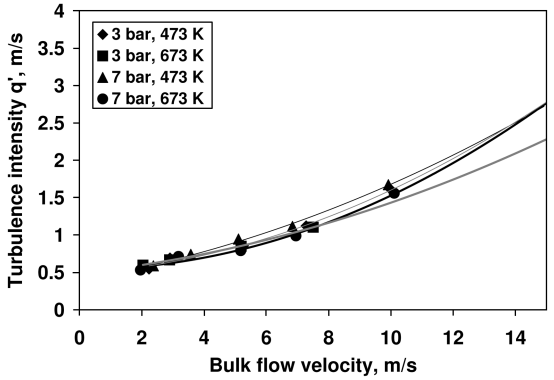

Fig. 8 Turbulence intensity q' measured at radial position $r = 12$ mm, depending on bulk gas flow velocity at different at different temperatures and pressures: 3 bara (gray), 7 bara (black).

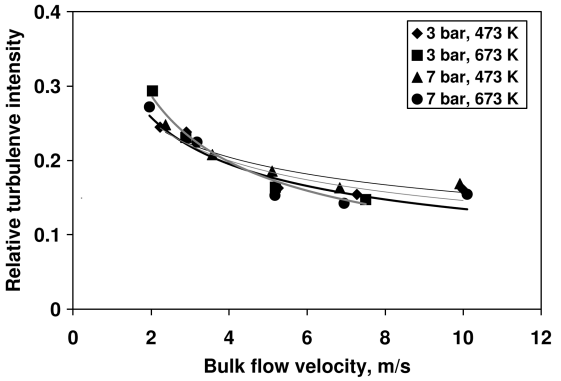

Fig. 9 The evolution of relative turbulence intensity $q'/\bar{u}$ depending on bulk gas flow velocity at different temperatures and pressures: 3 bara (gray), 7 bara (black).

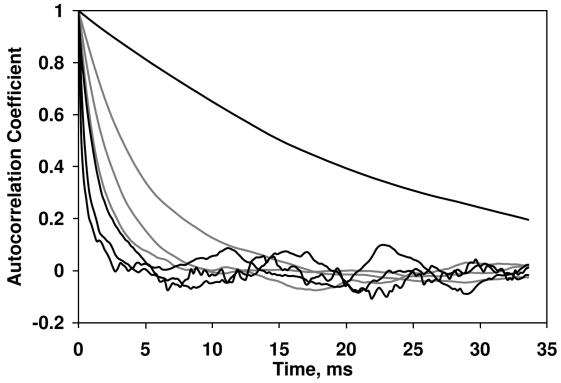

Fig. 10 Autocorrelation coefficient curves at burner radial position $r = 3$ mm for different gas flow velocities at 3 bara (gray) and 7 bara (black), 673 K.

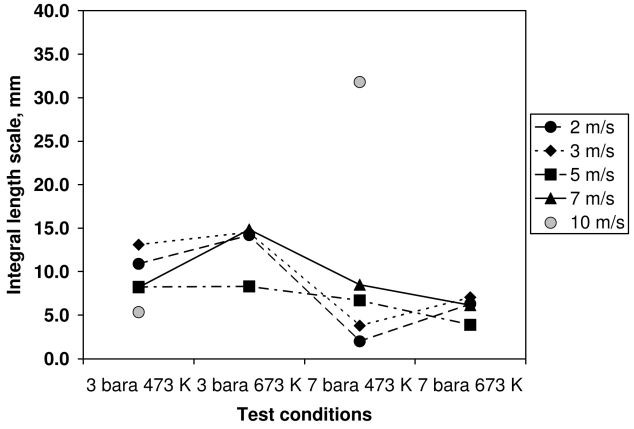

Fig. 11 Integral length scales measured 10 mm downstream burner at the burner centerline exit at 7 bara 673 K.

other exit velocities the increase in pressure reduces integral length scale slightly to 2.5–10 mm.

The differences in the integral length scale results appear to arise from a number of interacting factors. Although the mean axial velocity profiles follow well-known similarity trends, this is not so with the turbulence (Fig. 9), which clearly shows much higher levels of relative turbulence intensity at low bulk flow velocities with a somewhat weaker effect due to pressure and temperature. These results translate into the shown variation of integral length scale and seem to arise from variations in the jet potential core and the generated shear flow on its boundary. Reynolds number effects are clearly important, the lowest value being around 2400 (2 m/s, 3 bar, 673 K), up to 58,000 (10 m/s, 7 bar, 473 K), and do affect such jets in the lower Reynolds number ranges. Unfortunately, for such measurements it is impossible to obtain higher Reynolds numbers without the use of very much larger throughput rigs allowing larger diameter jets to be used.

B. Turbulent Burning Velocity

This study has investigated a range of flames at elevated temperatures and pressures. Laminar burning velocities, calculated using CHEMKIN, and Lewis numbers for different gas mixtures at different temperatures and pressures are presented in Table 2.

Only values close to the stoichiometric conditions are listed to show the variation trends of S_L and Lewis number.

For pure methane gas, the methane diffusion coefficient to the multicomponent mixture consisting of nitrogen and oxygen was calculated for lean mixtures. For rich mixtures oxygen diffusion to the mixture was calculated. For methane–carbon dioxide mixtures methane was taken as the deficient component for lean mixtures and oxygen for the rich ones. However, for methane–carbon dioxide mixtures the methane diffusion to the three-component mixture (nitrogen, oxygen, carbon dioxide) was assumed. For methane and hydrogen gases, methane and hydrogen were deficient species for lean mixtures and oxygen was the deficient gas for the rich mixtures.

Lewis number of methane for all equivalence ratios was close to unity for the conditions considered. Lewis number decreased slightly with the CO_2 addition compared with 100% methane. The most significant changes in Lewis number are observed for methane–hydrogen mixtures. Temperature and pressure had negligible effect on Lewis number.

To identify combustion regime, the flames studied under stoichiometric combustion are plotted on the Borghi diagram (Fig. 12). Turbulence intensity q', turbulent length scale l_0, obtained from our experiments (Figs. 8 and 11), and laminar flame thickness δ_L and laminar burning velocity S_L, obtained from CHEMKIN, have been used to calculate the data points. The graph shows that all the flames are within the corrugated flamelet regime. This is consistent with the aims of the project as it was undesirable to produce flames located in different regions of the Borghi diagram; for instance, higher temperatures may well have moved the operating regime to that of wrinkled flamelets.

A pilot flame was required to stabilize the main flame for some cases of lean methane–carbon dioxide mixtures and with lean methane for all pressures and temperatures. This pilot was switched off before taking images. Methane–hydrogen mixtures stabilized easily for all conditions, and the pilot flame was not required. The methane–hydrogen flames were found to be much more stable. No significant change in flame shape was noticed when comparing methane, methane–carbon dioxide, and methane–hydrogen mixtures,

Table 2 Experimental conditions and results of 100% methane, methane–carbon dioxide, and methane–hydrogen mixtures

CH_4			15%CO_2			30%CO_2			15%H_2			30%H_2		
Equivalence ratio	S_L	Le	Equivalence ratio	S_L	Le	Equivalence ratio	S_L	Le	Equivalence ratio	S_L	Le	Equivalence ratio	S_L	Le
3 bara 473 K														
1.18	0.52	1.106	1.21	0.41	1.096	1.20	0.33	1.083	1.22	0.54	1.145	1.24	0.61	1.194
0.96	0.56	0.948	1.04	0.50	1.096	1.02	0.41	1.084	1.00	0.62	0.725	1.01	0.71	1.178
0.75	0.37	0.954	0.71	0.29	0.951	0.74	0.27	0.944	0.82	0.48	0.724	0.90	0.63	0.593
7 bara 473 K														
1.20	0.32	1.106	1.39	0.14	1.096	1.18	0.21	1.083	1.23	0.32	1.145	1.23	0.40	1.193
1.01	0.39	1.105	1.20	0.26	1.096	0.99	0.27	0.935	1.06	0.42	1.139	0.99	0.48	0.596
0.78	0.24	0.953	0.81	0.25	0.948	0.76	0.18	0.944	0.86	0.34	0.724	0.85	0.39	0.592
3 bara 673 K														
1.14	1.16	1.104	1.25	0.86	1.094	1.17	0.82	1.081	1.19	1.23	1.139	1.25	1.30	1.187
1.04	1.20	1.103	1.03	1.07	1.094	1.03	0.91	1.082	1.02	1.31	1.134	0.99	1.46	0.595
0.73	0.82	0.948	0.79	0.86	0.942	0.74	0.68	0.937	0.82	1.08	0.722	0.82	1.21	0.591
7 bara 673 K														
-	-	-	1.19	0.67	1.094	1.20	0.52	1.081	1.22	0.81	1.140	1.22	0.93	1.186
-	-	-	1.04	0.76	1.094	1.01	0.63	1.082	1.03	0.94	1.134	1.01	1.03	1.172
-	-	-	0.77	0.56	0.942	0.78	0.50	0.936	0.79	0.69	0.722	-	-	-

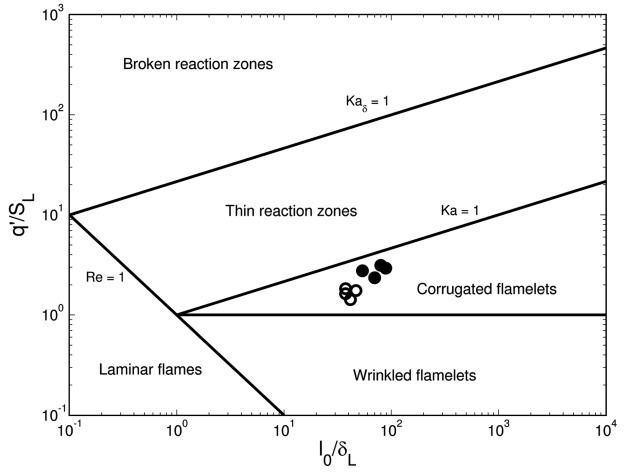

Fig. 12 Borghi–Peters diagram plotted on the logarithmic scale. Empty circles represent 3 bara 473 K, full circles represent 7 bara 473 K conditions; CH_4 gas, and CH_4-CO_2 and CH_4-H_2 mixtures.

although increased wrinkledness of the methane–hydrogen flames was observed, as anticipated [8].

1. Turbulent Burning Velocity Measurements

Turbulent burning velocity dependence on the equivalence ratio of different gas mixtures is presented in Figs. 13–16. Methane data are presented in all graphs as a benchmark indicator. The turbulent burning velocity S_T has been normalized by the methane turbulent burning velocity at $\phi = 0.96$, 3 bara, and 473 K, obtained in experiments. Trend lines are plotted through each data set. Only one test for each condition was conducted. The relative errors of the burning velocities, computed from the flame images, were below 1%; therefore, the error bar were not determined. The graphs are grouped so that the dependence of S_T on pressure (Figs. 13 and 15) and temperature (Figs. 14 and 16) can be shown. Normalized S_T of methane and methane–carbon dioxide mixtures are presented in Figs. 13 and 14, and methane and methane–hydrogen mixtures in Figs. 15 and 16.

The peak of S_T of methane is observed at $\phi = 1 - 1.1$ at all conditions. When the methane–air mixture at 3 bara is preheated to 673 K the burning velocity rises by approximately 55–60% in comparison with the methane burning velocity at 473 K at $\phi = 1$ (Fig. 13a). For $\phi = 1.2$ the increase in S_T is around 50%. At $\phi = 0.8$, 70% increase in S_T is observed at 3 bara pressure. The data consistently show that temperature has a stronger effect on S_T for lean mixtures than for rich.

Increasing ambient pressure from 3 to 7 bara at 473 K reduces methane turbulent burning velocity by approximately 15–20% at $\phi = 1$ (Fig. 14a). For the same temperature at $\phi = 1.2$ the increase in S_T is about 10%. Increased pressure has more influence for lean methane–air mixtures than is observed for rich ones.

The peaks of S_T of methane–carbon dioxide mixtures are observed at $\phi = 1 - 1.1$ at all conditions. For the higher temperatures, the peak of S_T is slightly shifted to richer mixtures. Small amounts of carbon dioxide added to methane did not change the mixture burning velocity significantly at 3 bara 473 K across all equivalence ratios (Fig. 13a). The turbulent burning velocity of 85%CH_4-15%CO_2 mixture remained virtually unchanged at this condition. However, a decrease in S_T by approximately 20% is measured at 3 bara 673 K for $\phi = 0.8$ (Fig. 13a) in comparison with pure methane. S_T of 85%CH_4-15%CO_2 for rich mixtures ($\phi > 1.1$) at 3 bara 673 K are slightly higher than S_T of pure methane. This implies that temperature effect on CO_2 enriched methane is stronger than for pure methane for rich mixtures ($\phi > 1.1$), whereas the converse holds for $\phi < 0.8$.

Thirty percent carbon dioxide content in methane reduced turbulent burning velocity. The burning velocity recorded for 70%CH_4-30%CO_2 was approximately 20–25% lower than that measured for pure methane at 3 bara 473 K at $\phi = 1$ (Fig. 13a).

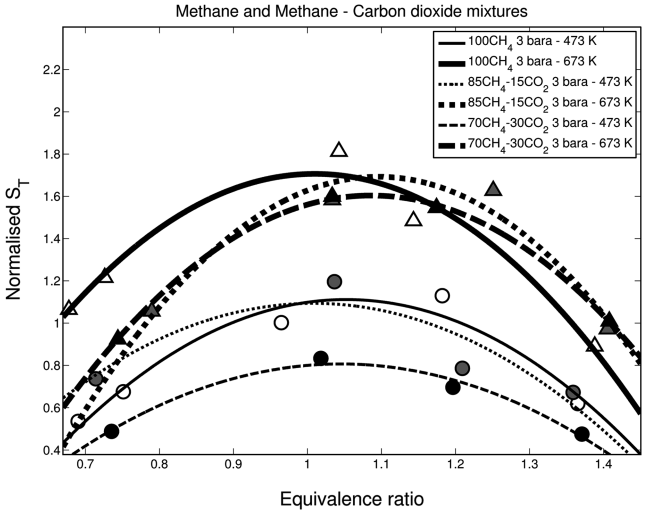

a)

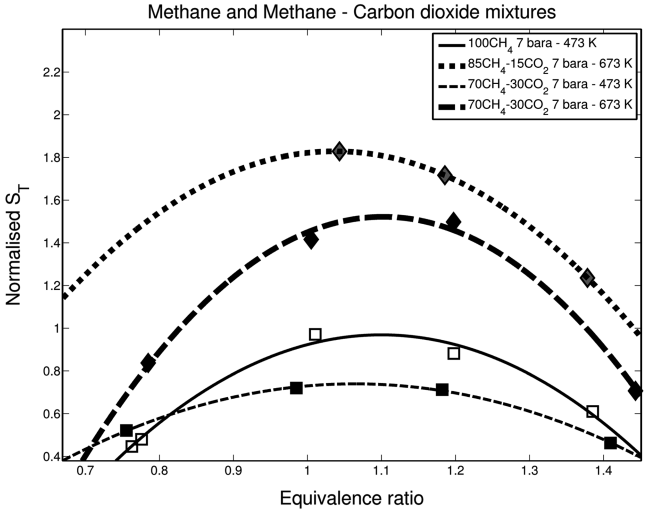

b)

Fig. 13 Normalized burning velocity of methane and methane–carbon dioxide mixtures at different pressures: a) 3 bara pressure, b) 7 bara pressure. Symbols: ○ represents 3 bara 473 K, △ represents 3 bara 673 K, □ represents 7 bara 473 K, ◇ represents 7 bara 673 K, blank represents CH_4, gray represents 85%CH_4-15%CO_2, and black represents 70%CH_4-30%CO_2.

Temperature increase had a bigger influence for 70%CH_4-30%CO_2, where burning velocity increased by 100–110% at 3 bara pressure at $\phi = 1$. At 3 bara 473 K the difference of S_T between methane and 70%CH_4-30%CO_2 was higher than at 3 bara 673 K (Fig. 13a), which supports the conclusion that the temperature effect on S_T is stronger for 70%CH_4-30%CO_2, and temperature effect rises with the increase of CO_2 content in methane.

The temperature increase raised the S_T of 85%CH_4-15%CO_2 by 60–70% at 3 bara pressure at $\phi = 1$ (Fig. 13a). However, an even larger increase of S_T by 70–80% was observed at 3 bara at $\phi = 1.2$. At 7 bara 673 K, the burning velocity of 85%CH_4-15%CO_2 is slightly higher than at 3 bara 673 K.

The S_T of 70%CH_4-30%CO_2 at 7 bara 673 K is lower than at 3 bara 673 K (Fig. 14b). However, the difference does not exceed 5% at $\phi = 1.1$. Thus, it can be concluded that there is a consistent trend for the effect of pressure on turbulent burning velocity of methane and methane–carbon dioxide mixtures. This is supported by the findings of other researchers who have been reported that increased pressure has little effect on the turbulent burning velocity of methane [11] and methane–carbon dioxide mixtures [7].

Hydrogen addition to methane increased the turbulent burning rate considerably (Fig. 15). Hydrogen addition also improved flame stability. It was noted that significantly leaner mixtures could be

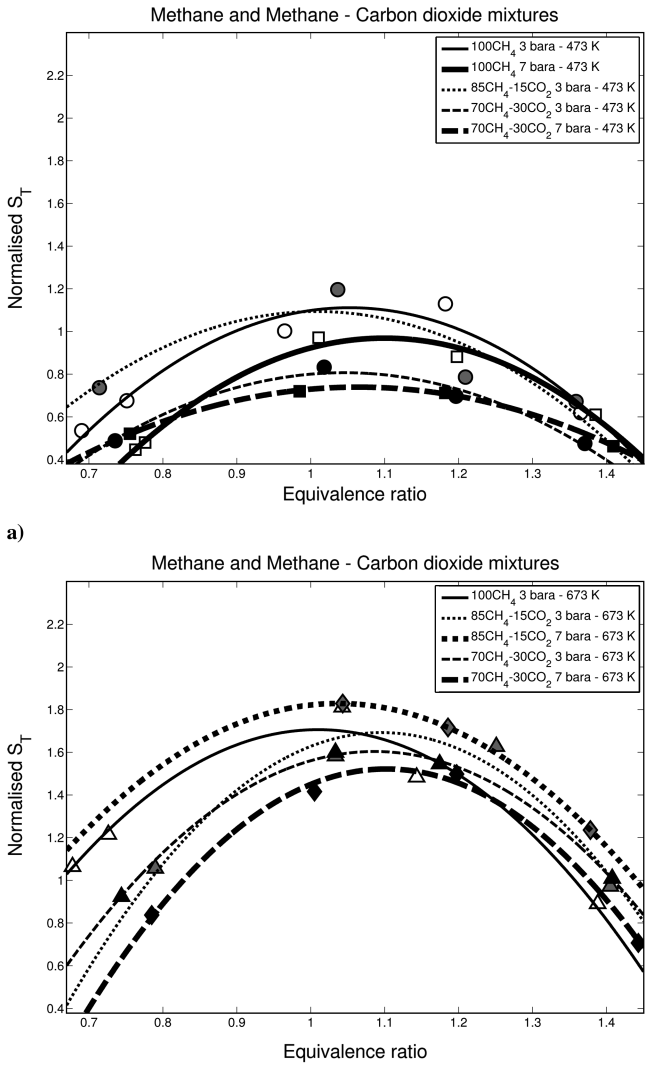

Fig. 14 Normalized burning velocity of methane and methane–carbon dioxide mixtures at different temperatures: a) 473 K temperature, b) 673 K temperature. Symbols: ○ represents 3 bara 473 K, △ represents 3 bara 673 K, □ represents 7 bara 473 K, ◇ represents 7 bara 673 K, blank represents CH_4, gray represents 85%CH_4-15%CO_2, and black represents 70%CH_4-30%CO_2.

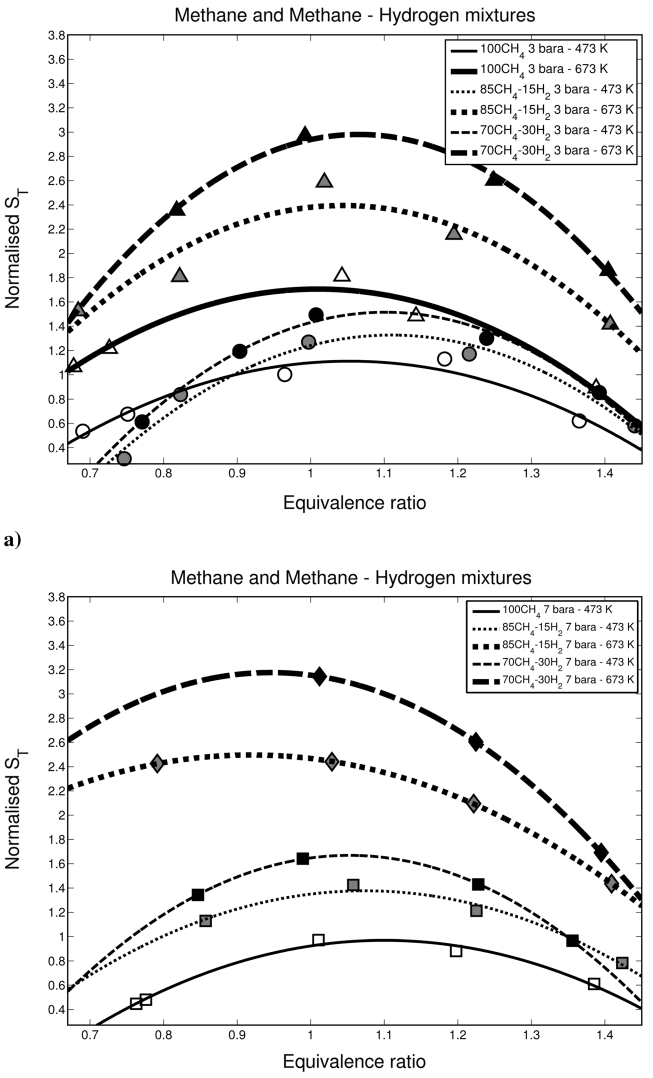

Fig. 15 Normalized burning velocity of methane and methane–hydrogen mixtures at different pressures. a) 3 bara pressure, b) 7 bara pressure. Symbols: ○ represents 3 bara 473 K, △ represents 3 bara 673 K, □ represents 7 bara 473 K, ◇ represents 7 bara 673 K, blank represents CH_4, gray represents 85%CH_4-15%H_2, and black represents 70%CH_4-30%H_2.

stabilized on the burner than was possible during the methane and methane–carbon dioxide experiments. Temperature increase also improved flame stability. These trends are expected, and similar to those reported by other researchers [5].

The peaks of S_T of methane–hydrogen mixtures are observed at $\phi = 1 - 1.1$ at 473 K temperature, however, the peaks are shifted to leaner mixtures at 673 K. Fifteen percent hydrogen addition increased burning velocity by approximately 20% for 3 bara 473 K at $\phi = 1$ in comparison with pure methane (Fig. 15). The increase of S_T at 3 bara 673 K at $\phi = 1$ was about 40–45% in comparison with pure methane (Fig. 15a). Thirty percent hydrogen addition increased turbulent burning velocity by up to 45–50% at 3 bara 473 K at $\phi = 1$ (Fig. 15) in comparison with pure methane. A larger increase of 80–90% of S_T was realized at 7 bara 473 K conditions at $\phi = 1$. The difference of S_T between 85%CH_4-15%H_2 and 70%CH_4-30%H_2 at 3 and 7 bara 473 K was about 15–20% (Fig. 16a), and about 25–30% at 3 and 7 bara 673 K for stoichiometric mixtures (Fig. 16b). Therefore, it implies that the augmentation of S_T of methane–hydrogen mixtures are more susceptible to temperature increase than for pure methane at stoichiometric conditions. The largest difference between burning velocity rates of methane and different methane–hydrogen mixtures was found to be around stoichiometric combustion conditions. On the fuel-rich side the difference becomes smaller. These trends are generally consistent with those reported by Mandilas et al. [8].

The effect of pressure increase from 3 to 7 bara was very small on S_T for 85%CH_4-15%H_2 at 473 and 673 K at $\phi = 1$ (Fig. 16). For rich mixtures the pressure effect at the same temperatures was negligible, however, the effect was more significant for lean mixtures. The burning velocity of 85%CH_4-15%H_2 at $\phi = 0.8$ increased by approximately 65% at 473 K, and by 40% at 673 K in comparison with S_T at 3 bara (Fig. 16). Similar trends were observed for 70%CH_4-30%H_2 mixture. The increase in pressure from 3 to 7 bara raised S_T for lean mixtures at 473 K and 673 K ambient temperatures.

For all methane–hydrogen mixtures at both 473 and 673 K, the increase in burning velocity due to ambient pressure increase is appreciable for lean mixtures (Fig. 16), whereas the burning velocity of rich methane—hydrogen mixtures is similar for both pressures and temperatures. Although there are insufficient data points to be fully confident of these trends and more detailed investigation is required, variation in turbulent burning characteristics with equivalence ratio and pressure have been reported elsewhere [9,23]. Variation in Markstein number and the influence of the preferential diffusion at different pressures and equivalence ratios are likely to play a significant role in explanation of such trends if consolidated.

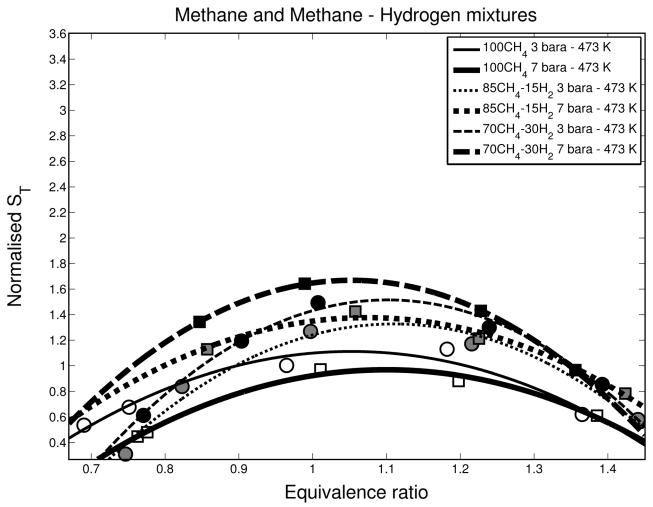

a)

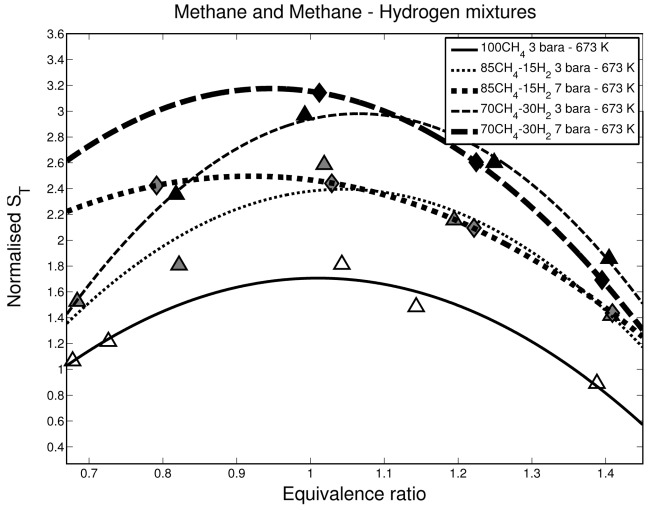

b)

Fig. 16 Normalized burning velocity of methane and methane–hydrogen mixtures at different pressures. a) 473 K temperature, b) 673 K temperature. Symbols: ○ represents 3 bara 473 K, △ represents 3 bara 673 K, □ represents 7 bara 473 K, ◇ represents 7 bara 673 K, blank represents CH_4, gray represents 85%CH_4-15%H_2, and black represents 70%CH_4-30%H_2.

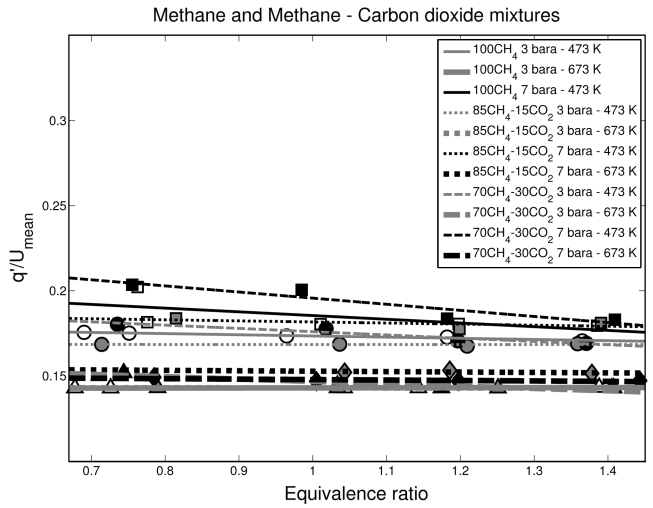

a)

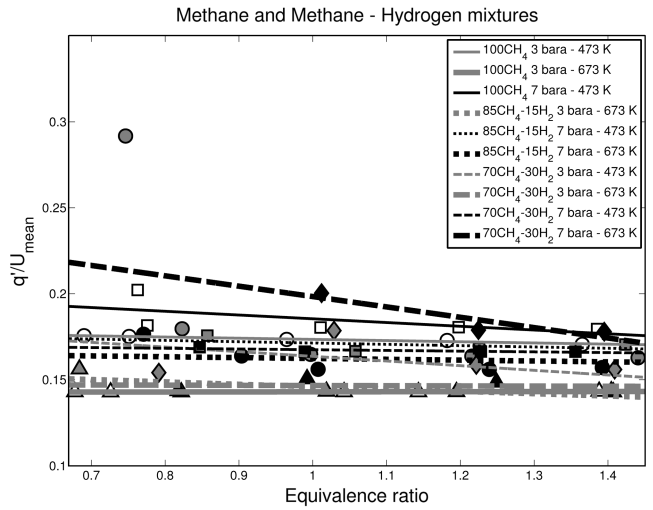

b)

Fig. 17 Relative turbulence intensity of methane, methane–carbon dioxide and methane–hydrogen mixtures. a) CH_4 and CH_4-CO_2 mixtures, b) CH_4 and CH_4-H_2 mixtures. Symbols: ○ represents 3 bara 473 K, △ represents 3 bara 673 K, □ represents 7 bara 473 K, ◇ represents 7 bara 673 K, blank represents CH_4, gray represents 85%CH_4-15%CO_2(H_2), and black represents 70%CH_4-30%CO_2(H_2).

2. *Relative Turbulence Intensity*

Methane, methane–carbon dioxide and methane–hydrogen mixtures relative turbulence intensities for different test conditions are plotted in Fig. 17. Relative turbulence intensity is represented as turbulence intensity normalized by mean velocity $q'/\bar{u}$. Blank symbols in the graphs represent pure methane data points, gray symbols 85% methane–15% additional gas mixture data points, and full black symbols 70% methane–30% additional gas mixture data points. The graphs are presented to indicate the variation in turbulence characteristics during the experiment. Different bulk gas exit velocities were used during the tests, thus giving some variation in absolute values of $\bar{u}$, q', and relative turbulence intensity.

Relative turbulence intensity remained broadly constant, at around 14–18%, for methane, 85%CH_4-15%CO_2, and 70%CH_4-30%CO_2 for most test conditions (Fig. 17a). For pure methane at 7 bara 473 K, the relative turbulence intensity is slightly higher, at around 19%. Variable $q'/\bar{u}$ is observed for 70%CH_4-30%CO_2, also at 7 bara 473 K. Here $q'/\bar{u}$ drops from 20% for lean mixtures to 18% for rich mixtures. This is due to the higher bulk exit velocity of the gas mixture required to stabilize rich mixtures during the experiments. For 70%CH_4-30%CO_2 at 7 bara 473 K at $\phi = 0.76$, very low bulk exit velocity at $\bar{u} = 3.5$ m/s has been maintained to keep the slow burning gas flame stable. Thus, the $q'/\bar{u}$ increased to 20%. For methane $\phi = 0.78$ at the same condition the velocity $\bar{u} = 4.9$ m/s was maintained, therefore, $q'/\bar{u}$ was lower. In general for all lean mixtures the velocity had to be slightly reduced to stabilize the flame.

Similar trends have been observed for 85%CH_4-15%H_2 and 70%CH_4-30%CO_2 (Fig. 17b). Relative turbulence intensity was constant in the majority of tests undertaken for methane–hydrogen mixtures. Only for 85%CH_4-15%H_2 at 3 bara 473 K and 70%CH_4-30%H_2 at 7 bara 673 K are the variations significant. This is due to a very low gas mixture exit velocity of $\bar{u} = 2$ m/s for 85%CH_4-15%H_2 at $\phi = 0.75$, 3 bara 473 K being used, thus increasing the relative turbulence intensity. As for methane–carbon dioxide mixtures, generally the relative turbulence intensity was around 14–18%. At lower temperature conditions $q'/\bar{u}$ values are higher, because the exit velocity required for flame stabilization is lower.

3. *Data Comparison and Correlation*

The comparison of experimental results with the findings of other researchers and turbulent combustion models are discussed here.

Comparison of methane experiment results with the Peters [24] and Zimont et al. [25] correlations and the data from Kobayashi et al. [14] and Filatyev et al. [16] is presented in Fig. 18. Griebel et al. [11]

report that the Peters [24] and Zimont et al. [25] correlations overpredict their data, where flames are within the thin reaction zone regime. Our results, within the corrugated flamelet regime, with l_0/δ_L in the range of 60–100, are closer to the Peters' correlation, although as for Griebel et al. [11], they are also overpredicted by the Peters' predictions. Correlations for Zimont et al. [25] are plotted for elevated temperature and pressure for different integral length scales l_0.

Kobayashi et al. [14] performed similar measurements for methane–air flames at elevated temperature and pressures. Consistent with the work reported here, the flames studied fell into the corrugated regime on the Borghi diagram making the results of Kobayashi et al. [14] a useful comparison. As observed from Fig. 18, the turbulent and laminar burning velocity ratio recorded by Kobayashi et al. [14] is higher than the current results. Their data is also significantly underpredicted by Peters' correlation despite the fact it was seen to overpredict the measurements reported here, as well as those by Griebel et al. [11] and Filatyev et al. [16].

One possible explanation for these discrepancies could be the different interpretation methods of processed flame images. Kobayashi et al. [14] has calculated flame areas from contours obtained at progress variable value 0.1. This means that smaller flame areas have been derived and, therefore, higher burning velocities obtained, compared with those obtained from progress variable value 0.5, which the authors contend represents the averaged flame contour more accurately. The difference in image processing techniques employed may also account for some of the difference; here the single image processing technique is used, whereas Kobayashi et al. [14] used the average image processing technique.

Another comparison with Filatyev et al. [16] experiments is presented in Fig. 18. Filatyev et al. [16] have performed experiments in a slot type burner at 1 bara 296 K ambient conditions. The relative turbulence intensity in their experiment is 20%, which is very close to the conditions in this study. Filatyev et al. [16] argue that turbulent burning velocity depends on mean velocity $\bar{u}$ and burner width, or in other words, on burner geometry. They also propose that Bunsen burner flames should display a nonlinear dependence (bending effect). A slightly higher value of S_T/S_L at 7 bara 473 K is observed in the graph. This observation could imply that pressure affects turbulent and laminar burning velocity ratio as indeed has been reported by other researchers [3,14].

In Fig. 19 a comparison of the turbulent and laminar burning velocity ratio from this test program and the Kobayashi et al. [4] findings are presented. The data of Kobayashi et al. [4] for methane and methane–carbon dioxide mixtures are consistently higher than

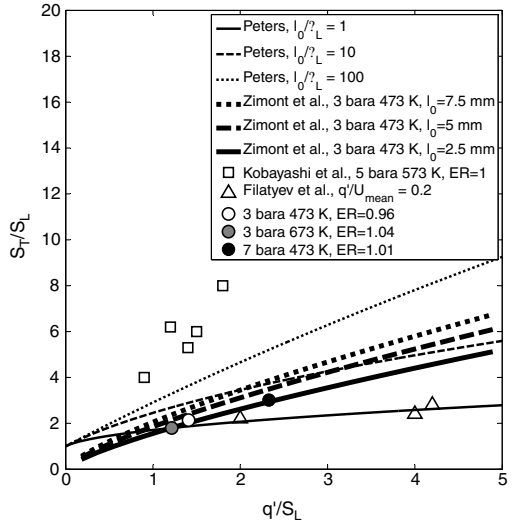

Fig. 18 Comparison of methane turbulent and laminar burning velocities ratio S_T/S_L of our experiments with Peters [24] and Zimont et al. [25] at different lengthscale ratios l_0/δ_L and different integral length scales l_0, and Kobayashi et al. [14] and Filatyev et al. [16] experiments data.

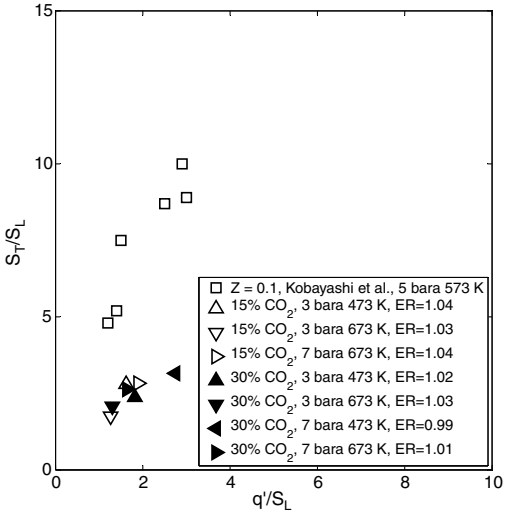

Fig. 19 Comparison of methane–carbon dioxide mixtures turbulent and laminar burning velocity ratio S_T/S_L of our experiments with Kobayashi et al. [14] experiment data at elevated temperature and pressure. In the experiments, CO_2 was diluted in air, $Z = X_{CO_2}/(X_{air} + X_{CO_2})$.

the current experiments, with contributory reasons for these findings discussed earlier. The effect of carbon dioxide addition has been reported by Kobayashi et al. [4]. They found that the ratio of turbulent to laminar burning rate and mean fuel consumption rate decreased with increasing CO_2 dilution ratio. A possible explanation is offered by the effect of increased Markstein length [4], which means that local burning velocity in the turbulent flame region decreases with local stretch due to turbulence. Another possible influence considered concerns variation of the smallest wrinkling scale of a $CH_4/air/CO_2$ flame, which was smaller than that of the flame with no CO_2 dilution.

The comparison of the methane–hydrogen results from this program with those of Shy et al. [7] and Kido et al. [9] are presented in Figs. 20 and 21. Shy et al. [7] performed their experiments at atmospheric conditions and show that the trends for S_T/S_L as a function of q'/S_L are in reasonable agreement with ours (Fig. 20). The same trends are reported for pure hydrogen in the paper of Kitagawa et al. [23]. Figure 21 presents the turbulent burning velocity reported by Kido et al. [9] (after normalizing the data by the methane burning velocity at 3 bara 473 K at $\phi = 0.96$). The Kido et al. [9] experiments were undertaken utilizing propagating flames.

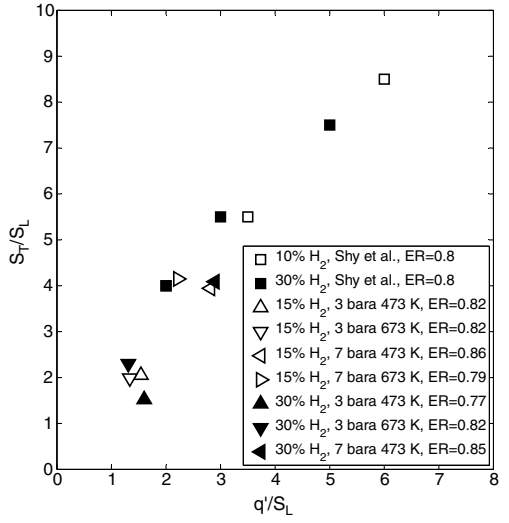

Fig. 20 Methane–hydrogen mixtures turbulent burning velocity comparison of our experiments with Shy et al. [7]. Turbulent burning velocity data normalized by laminar burning velocity.

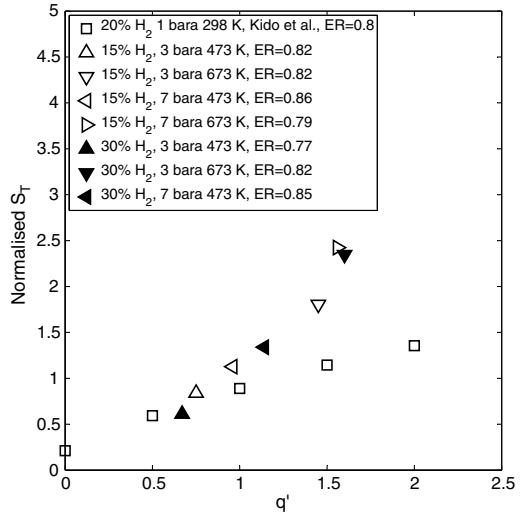

Fig. 21 Methane–hydrogen mixtures turbulent burning velocity comparison of our experiments with Kido et al. [9]. These results of turbulent burning velocity are normalized by methane burning velocity at 3 bara 473 K at $\phi = 0.96$ obtained in our experiments.

The current data correlates well with their findings for q' less than 1. For higher q' the differences are noticeable. This implies that both temperature and pressure have a strong effect on S_T, and this effect arises from differences both in the type of flames and especially the turbulence characteristics of a propagating as opposed to that of a conical shape flame.

IV. Conclusions

1) Investigations of turbulent burning velocity of gaseous alternative fuels at elevated pressure and temperature have been undertaken in a new large-scale HPOC facility. Methane, methane–carbon dioxide, and methane–hydrogen mixtures have been tested across a broad range of equivalence ratio with pressures up to 7 bar and inlet temperature up to 673 K. All flames considered have been chosen in the corrugated flamelet regime, through appropriate choice of operating conditions.

2) An alternative analysis method for turbulent flame image processing and hence turbulent burning velocity calculation has been proposed and applied. The results have been assessed against other commonly used methodologies, and although the method proved to be reliable in this program, further investigation and refinement is ongoing.

3) Methane and methane–carbon dioxide mixtures turbulent burning velocity results have been compared with Peters [24] and Zimont et al. [25] correlations and recent data of Kobayashi et al. [14] and Filatyev et al. [16]. The results show reasonable agreement with Peters' predictions. However, the results show differences with the findings of Kobayashi et al. [14], most likely due to data analysis differences such as the selected value of progress variable.

4) Methane–hydrogen mixture results correlate well with recent data from Shy et al. [7], who used the alternative propagating flame method for quantifying turbulent burning velocity, notwithstanding differences in pressure and temperature between data sets.

5) These data quantify the reduction in turbulent burning rate induced by carbon dioxide addition to methane for a variety of equivalence ratios. Increase in initial ambient gas temperature significantly increases turbulent burning velocity, whereas increase in ambient pressure induces a reduction. Methane and methane–carbon dioxide mixtures demonstrate similar trends with respect to the influence of ambient conditions.

6) Hydrogen addition to methane has been found to considerably increase turbulent burning velocity even for small volumes of hydrogen addition. For lean hydrogen–methane mixtures, an increase in temperature or pressure augments turbulent burning velocity, whereas the influence of ambient pressure is minimal for rich mixtures.

Acknowledgments

This research was financed by the European Comission under their Alternative Fuels for Industrial Gas Turbines project (ENK5-CT-2002-00662). A.B. thanks the European Union for sponsoring his research under the Marie Curie program Inegrated Energy Conversion for Sustainable Environment (MEST-CT-2005-021018). The authors thank Gas Turbine Research Centre Facility Manager S. Morris for helping to perform experiments and T. Treherne and P. Malpas for technical assistance.

References

[1] Gökalp, I., and Lebas, E., "Alternative Fuels for Industrial Gas Turbines (AFTUR)," *Applied Thermal Engineering*, Vol. 24, Nos. 11–12, 2004, pp. 1655–1663. doi:10.1016/j.applthermaleng.2003.10.035

[2] Egolfopoulus, F. N., Cho, P., and Law, C. K., "Laminar Flame Speeds of Methane-Air Mixtures Under Reduced and Elevated Pressures," *Combustion and Flame*, Vol. 76, Nos. 3–4, 1989, pp. 375–391. doi:10.1016/0010-2180(89)90119-3

[3] Kobayashi, H., "Experimental Study of High-Pressure Turbulent Premixed Flames," *Experimental Thermal and Fluid Science*, Vol. 26, Nos. 2–4, 2002, pp. 375–387. doi:10.1016/S0894-1777(02)00149-8

[4] Kobayashi, H., Hagiwara, H., Kaneko, H., and Ogami, Y., "Effects of CO_2 Dilution on Turbulent Premixed Flames at High Pressure and High Temperature," *Proceedings of the Combustion Institute*, Vol. 31, 2007, pp. 1451–1458. doi:10.1016/j.proci.2006.07.159

[5] Griebel, P., Boschek, E., and Jansohn, P., "Lean Blowout Limits and NO_x Emissions of Turbulent, Lean, Premixed, Hydrogen-Enriched Methane/Air Flames at High Pressure," *Journal of Engineering for Gas Turbines and Power*, Vol. 129, No. 2, 2007, pp. 404–410. doi:10.1115/1.2436568

[6] Halter, F., Chauveau, C., and Gökalp, I., "Characterization of the Effects of Hydrogen Addition in Premixed Methane/Air Flames," *International Journal of Hydrogen Energy*, Vol. 32, No. 13, 2007, pp. 2585–2592. doi:10.1016/j.ijhydene.2006.11.033

[7] Shy, S., Chen, Y. C., Yang, C. H., Liu, C. C., and Huang, C. M., "Effects of H_2 or CO_2 Addition, Equivalence Ratio, and Turbulent Straining on Turbulent Burning Velocities for Lean Premixed Methane Combustion," *Combustion and Flame*, Vol. 153, No. 4, 2008, pp. 510–524. doi:10.1016/j.combustflame.2008.03.014

[8] Mandilas, C., Ormsby, M. P., Sheppard, C. G. W., and Wooley, R., "Effects of Hydrogen Addition on Laminar and Turbulent Premixed Methane and Iso-Octane-Air Flames," *Proceedings of the Combustion Institute*, Vol. 31, 2007, pp. 1443–1450. doi:10.1016/j.proci.2006.07.157

[9] Kido, H., Nakahara, M., Hashimoto, J., and Barat, D., "Turbulent Burning Velocities of Two-Component Fuel Mixtures of Methane, Propane and Hydrogen," *JSME International Journal Series B*, Vol. 45, No. 2, 2002, pp. 355–362.

[10] Natarajan, J., Lieuwen, T., and Seitzman, J., "Laminar Flame Speeds of H_2/CO Mixtures: Effect of CO_2 Dilution, Preheat Temperature, and Pressure," *Combustion and Flame*, Vol. 151, Nos. 1–2, 2007, pp. 104–119. doi:10.1016/j.combustflame.2007.05.003

[11] Griebel, P., Bombach, R., Inauen, A., Schären, R., Schenker, S., and Siewert, P., "Flame Characteristics and Turbulent Flame Speeds of Turbulent, High-Pressure, Lean Premixed Methane/Air Flames," *ASME Turbo Expo 2005: Power for Land, Sea and Air*, Vol. 2, American Society of Mechanical Engineers, Fairfield, NJ, 2005.

[12] Griebel, P., Siewert, P., and Jansohn, P., "Flame Characteristics of Turbulent Lean Premixed Methane/Air Flames at High Pressure: Turbulent Flame Speed and Flame Brush Thickness," *Proceedings of the Combustion Institute*, Vol. 31, No. 2, 2007, pp. 3083–3090. doi:10.1016/j.proci.2006.07.042

[13] Pfadler, S., Leipertz, A., and Dinkelacker, F., "Systematic Experiments on Turbulent Premixed Bunsen Flames Including Turbulent Flux Measurements," *Combustion and Flame*, Vol. 152, No. 4, 2008, pp. 616–631. doi:10.1016/j.combustflame.2007.11.006

[14] Kobayashi, H., Seyama, K., Hagiwara, H., and Ogami, Y., "Burning Velocity Correlation of Methane/Air Turbulent Premixed Flames at High Pressure and High Temperature," *Proceedings of the Combustion Institute*, Vol. 30, 2005, pp. 827–834. doi:10.1016/j.proci.2004.08.098

[15] Bilger, R. W., Pope, S. B., Bray, K. N. C., and Driscoll, J. F., "Paradigms in Turbulent Combustion Research," *Proceedings of the Combustion Institute*, Vol. 30, 2005, pp. 21–42. doi:10.1016/j.proci.2004.08.273

[16] Filatyev, S. A., Driscoll, J. F., Carter, C. D., and Donbar, J. M., "Measured Properties of Turbulent Premixed Flames for Model Assessment, Including Burning Velocities, Stretch Rates, and Surface Densities," *Combustion and Flame*, Vol. 141, Nos. 1–2, 2005, pp. 1–21. doi:10.1016/j.combustflame.2004.07.010

[17] Cheng, R. K., and Shepherd, I. G., "The Influence of Burner Geometry on Premixed Turbulent Flame Propagation," *Combustion and Flame*, Vol. 85, Nos. 1–2, 1991, pp. 7–26. doi:10.1016/0010-2180(91)90174-A

[18] Driscoll, J. F., "Turbulent Premixed Combustion: Flamelet Structure and its Effect on Turbulent Burning Rate," *Progress in Energy and Combustion Science*, Vol. 34, No. 1, 2008, pp. 91–134. doi:10.1016/j.pecs.2007.04.002

[19] Lafay, Y., Renou, B., Cabot, G., and Boukhalfa, M., "Experimental and Numerical Investigation of the Effect of H_2 Enrichment on Laminar Methane-Air Flame Thickness," *Combustion and Flame*, Vol. 153, No. 4, 2008, pp. 540–561. doi:10.1016/j.combustflame.2007.10.002

[20] Lachaux, T., Halter, F., Chauveu, C., Gökalp, I., and Shepherd, I. G., "Flame Front Analysis of High-Pressure Turbulent Lean Premixed Methane-Air Flames," *Proceedings of the Combustion Institute*, Vol. 30, 2005, pp. 819—826. doi:10.1016/j.proci.2004.08.191

[21] Hinze, J. O., *Turbulence*, McGraw–Hill, New York, 1975.

[22] Chen, Y. C., and Bilger, R. W., "Simultaneous 2-D Imaging Measurements of Reaction Progress Variable and OH Radical Concentration in Turbulent Premixed Flames: Experimental Methods and Flame Brush Structure," *Combustion Science and Technology*, Vol. 167, No. 1, 2001, pp. 131–167. doi:10.1080/00102200108952180

[23] Kitagawa, T., Nakahara, T., Maruyama, K., Kado, K., Hayakawa, A., and Kobayashi, S., "Turbulent Burning Velocity of Hydrogen-Air Premixed Propagating Flames at Elevated Pressures," *International Journal of Hydrogen Energy*, Vol. 33, No. 20, 2008, pp. 5842–5849. doi:10.1016/j.ijhydene.2008.06.013

[24] Peters, N., "The Turbulent Burning Velocity for Large-Scale and Small-Scale Turbulence," *Journal of Fluid Mechanics*, Vol. 384, 1999, pp. 107–132. doi:10.1017/S0022112098004212

[25] Zimont, V., Polifke, W., Bettelini, M., and Weisenstein, W., "An Efficient Computational Model for Premixed Turbulent Combustion at High Reynolds Numbers Based on a Turbulent Flame Speed Closure," *Journal of Engineering for Gas Turbines and Power*, Vol. 120, No. 3, 1998, pp. 526–532. doi:10.1115/1.2818178

E. Gutmark
Associate Editor